



## **Coated stainless steel 441 as interconnect material for solid oxide fuel cells: Evolution of electrical properties**

Downloaded from: <https://research.chalmers.se>, 2025-12-10 01:14 UTC

Citation for the original published paper (version of record):

Grolig, J., Froitzheim, J., Svensson, J. (2015). Coated stainless steel 441 as interconnect material for solid oxide fuel cells: Evolution of electrical properties. *Journal of Power Sources*, 284: 321-327.  
<http://dx.doi.org/10.1016/j.jpowsour.2015.03.029>

N.B. When citing this work, cite the original published paper.



# Coated stainless steel 441 as interconnect material for solid oxide fuel cells: Evolution of electrical properties



Jan Gustav Grovig\*, Jan Froitzheim, Jan-Erik Svensson

Environmental Inorganic Chemistry, Chalmers University of Technology, Kemivägen 10, SE-41296 Göteborg, Sweden

## HIGHLIGHTS

- We exposed cerium/cobalt coated AISI 441 in a SOFC cathode side atmosphere.
- We tested two different methods of ASR measurement.
- In-situ measured samples were heavily affected by platinum electrodes.
- ASR values of ex-situ measured samples could be related to oxidation.
- The oxidation and chromium volatilization were monitored.

## ARTICLE INFO

### Article history:

Received 9 January 2015  
Received in revised form  
20 February 2015  
Accepted 4 March 2015  
Available online 5 March 2015

### Keywords:

ASR  
Interconnect  
AISI 441  
SOFC  
Corrosion  
Platinum

## ABSTRACT

AISI 441 coated with a double layer coating of 10 nm cerium (inner layer) and 630 nm cobalt was investigated and in addition the uncoated material was exposed for comparison. The main purpose of this investigation was the development of a suitable ASR characterization method. The material was exposed to a simulated cathode atmosphere of air with 3% water at 850 °C and the samples were exposed for up to 1500 h. We compared two methods of ASR measurements, an in-situ method where samples were measured with platinum electrodes for longer exposure times and an ex-situ method where pre-oxidized samples were measured for only very short measurement times. It was found that the ASR of ex-situ characterized samples could be linked to the mass gain and the electrical properties could be linked to the evolving microstructure during the different stages of exposure. Both the degradation of the electric performance and the oxygen uptake (mass gain) followed similar trends. After about 1500 h of exposure an ASR value of about 15 mΩcm<sup>2</sup> was reached. The in-situ measured samples suffered from severe corrosion attack during measurement. After only 500 h of exposure already a value of 35 mΩcm<sup>2</sup> was obtained.

© 2015 The Authors. Published by Elsevier B.V. This is an open access article under the CC BY-NC-ND license (<http://creativecommons.org/licenses/by-nc-nd/4.0/>).

## 1. Introduction

Solid oxide fuel cells are seen as a key element in future energy and heat production. Due to their large versatility they can be used both in stationary, for example CHP applications, but also in mobile applications, such as auxiliary power units. Several fuel cell units need to be stacked to reach sufficient power densities and so-called interconnects are needed connect two adjacent fuel cell elements.

Improvements in electrode and electrolyte performance have led to lower operational temperatures, which allow the use of metallic interconnects [1–3]. There has been extensive research on

the development of suitable alloys, which have to have a similar coefficient of thermal expansion (CTE) compared to the ceramic fuel cell elements, a good high temperature stability and that form reasonable electrical conductive oxide scales. Examples of these alloys are Crofer 22 H, Crofer 22 APU, Sanergy HT or ZMG 232 [4–6]. Other alloys that have not been specially developed for fuel cell applications, such as AISI 441 or AISI 430, have also been investigated [1,7–9]. All of the alloys mentioned are ferritic stainless steels that form chromium-containing oxide scales, which protect the steel from rapid oxidation.

With respect to the interconnect one can identify three major factors that are detrimental for the SOFC performance; the oxidation of the steel, the evaporation of chromium and an increasing electrical resistance due to the oxide scale formation.

The oxidation of the interconnect on both the anode and

\* Corresponding author.

E-mail address: [jan.grovig@chalmers.se](mailto:jan.grovig@chalmers.se) (J.G. Grovig).

cathode side leads during long term operation to a depletion of chromium – which then allows enhanced oxidation and finally leads to mechanical disintegration. Oxidation of the steel can usually be quantified by gravimetry, which is proportional to the oxygen uptake, if no spallation or evaporation processes are involved.

Due to the water vapor present in the cathode atmosphere, the chromium-rich oxide scale evaporates a small amount of chromic species ( $\text{CrO}_2(\text{OH})_2$ ), which then react at the cathode/electrolyte/air triple points. This is known as cathode poisoning and is another detrimental factor for the fuel cell performance [10,11]. A relatively new technique for chromium evaporation measurement was developed at Chalmers University of Technology and allows the time-resolved quantification of evaporated chromium for different samples [12].

The growing oxide scale finally leads to an increased electrical resistance across the interconnect. A common way of expressing the electrical resistance is using the term area specific resistance (ASR). This is the cross plane resistivity given in  $\text{m}\Omega \times \text{cm}^2$ , which allows the comparison of different interconnect materials, without additional calculation steps for different oxide scale thicknesses.

Additional coatings are a common way to reduce the above mentioned issues and to improve the interconnect performance with regard to corrosion, chromium evaporation and electrical resistance [13]. The coatings vary in thickness and composition. A compilation of coatings for interconnects can be found in our previous study on improving corrosion properties and mitigating chromium evaporation of AISI 441 by the use of nanometer thick coatings. There it was found that both lifetime and chromium evaporation could be significantly improved by the application of an additional coating of cerium and cobalt [1]. However no data on the ASR evolution was reported, but will be presented in this work.

The characterization of the area specific resistance (ASR) is complicated by a number of issues, in particular contacting. Different methods have been developed, which can be differentiated by the material that is used for contacting the oxide scale. All methods usually have in common that the ASR is considered to be determined by the growing oxide scale and the resistance of the steel itself is neglected. The ASR can be usually expressed as shown in equation (1) [14]:

$$\text{ASR}_{\text{Interconnect}} = \rho \cdot \tau \quad (1)$$

where  $\rho$  is the specific resistivity of the oxide scale and  $\tau$  is the oxide scale thickness. The ASR is usually given in  $\text{m}\Omega \text{cm}^2$ . In case of a double layered oxide scales consisting of an inner chromia layer and an outer spinel layer usually found on SOFC interconnect steels the relationship expands to:

$$\text{ASR}_{\text{Interconnect}} = \rho_{\text{chromia}} \cdot \tau_{\text{chromia}} + \rho_{\text{spinel}} \cdot \tau_{\text{spinel}} \quad (2)$$

Taking into account that the specific resistivity is more or less constant during exposure and in case of a coated interconnect, highly conductive spinels are used as coating material; one can assume that the ASR value is almost directly related to the chromia thickness. Thus the ASR should be proportional to the mass gain of the steel.

The contact materials used for ASR characterization can be classified into noble metals such as platinum, gold or silver, which are not supposed to react or influence the oxidation behavior, and contacts, which are used in solid oxide fuel cell cathodes such as LSM ( $\text{La}_{1-x}\text{Sr}_x\text{MnO}_3$ ) or LSC ( $\text{LaSrCoO}$ ) [9,15–22]. Both have advantages and disadvantages. Noble metals that are not reacting with the oxide material give a more theoretical view of the conductivity evolution, whereas SOFC cathode materials simulate more

realistically how the ASR is expected to evolve in a real fuel cell stack. A problem with using noble metals as contact material is often in achieving a reasonable thickness of electrode and therefore metal pastes, which are applied as contacts, have been a common way to apply these electrodes. These pastes often sinter during the initial part of the high temperature exposure, which affects the ASR values [23,24]. In cases where LSM or LSC is used one has also encountered sintering effects in the early stages of exposure, the contact area is undefined, and there is a higher electrode resistance and also contact resistance [15,25]. Additionally interactions between the electrodes with the interconnect steels have been reported [26].

## 2. Experimental

### 2.1. Sample preparation

Pre-coated steel sheets with 0.2 mm thickness of AISI 441 (composition given in Table 1) were obtained from Sandvik Materials Technology AB. The sheets were manually cut into coupons of  $15 \times 15 \text{ mm}^2$ . The coating was applied at Sandvik Materials Technology using an industrially available PVD coating process. Metallic targets were used to produce the double layer coating which consists of an inner coating of 10 nm cerium and an outer layer of 630 nm cobalt. The samples were ultrasonically cleaned in two steps, first in acetone and then in ethanol, and finally the samples were weighed using a Sartorius MC5 scale.

### 2.2. Exposure

The samples were exposed using the denuder technique and tubular furnaces with a temperature of  $850^\circ\text{C}$  and an absolute humidity of 3% water content were used. The air flow was set to a value of 6 l/min, which is equal to 27 cm/s and which was proven in previous works to be in the flow independent regime of chromium evaporation [12]. Details on the exposure setup can be found in Ref. [1]. Samples were exposed both isothermally (no cool-down until the end of the exposure) and discontinuous (several interruptions with weighing in-between) for up to 1500 h.

### 2.3. Area specific resistance measurements

We used a new approach to produce area-defined electrodes of platinum to measure the ASR. A sputter mask of  $10 \times 10 \text{ mm}^2$  was placed on a pre-oxidized sample, and the sample was then sputtered with platinum for 10 min using a Quorum 150 sputter coater and a sputter current of 60 mA. This procedure was then repeated for the reverse-side of the sample. The sputtering step was used in order to produce electrodes with a defined area and to avoid direct contact of the platinum paste with the sample surface. After sputtering, the electrodes were re-painted with platinum paste (Metalor 6082) using a fine brush. To remove the binder from the platinum paint, the samples were fired at  $850^\circ\text{C}$  in air with a peak time of 10 min. To investigate the time-dependent evolution of the ASR different pre-oxidation times up to 1500 h were used. Additionally a few samples were measured after a pre-oxidation time of only 60 min for up to 500 h – below referred as in-situ samples.

A Probostat (NorECs, Norway) test cell, placed in a tubular

**Table 1**

Batch-specific values provided by the manufacturer, given in wt. %.

	Fe	Cr	C	Mn	Si	S	P	Ni	Nb	Ti
Wt. %	Bal.	17.83	0.012	0.26	0.55	0.002	0.024	0.13	0.48	0.14

furnace, was used to connect the sample to a Solartron 1260A impedance analyzer. The resistance of each sample was measured at temperatures between 900 and 500 °C. The impedance analyzer was run at a frequency of 1 Hz, and at each temperature the ASR was measured several times. Since the frequency was relatively low, the measurement was considered to be a quasi-DC measurement. The measured values were divided by 2 to obtain the ASR for one oxide scale.

### 3. Results

#### 3.1. Gravimetric measurements

The mass gain of the cerium cobalt coated samples compared to uncoated substrate material is plotted in Fig. 1. It can be clearly seen that the coated material had a very rapid high initial mass gain of about 0.21 mg/cm<sup>2</sup> after only about 100 min. This effect is due to the conversion/oxidation of the metallic cobalt top coating to cobalt oxide, as it was shown in previous studies [27]. After this initial oxidation step the mass gain of the coated samples followed an almost parabolic trend. After a total exposure time of 1500 h a mass gain of 0.85 mg/cm<sup>2</sup> was recorded for the coated material and the oxide scale was well adherent. Isothermal and discontinuous exposed coated samples did not differ significantly in mass gain when exposed for similar times.

In contrast to the coated material, the uncoated material suffered from severe spallation, especially after several cooling down cycles and longer exposure times, which is also reflected in the larger error bars. A total mass gain of  $0.54 \pm 0.15$  mg/cm<sup>2</sup> was observed for the uncoated material after 1150 h. Additionally one has to keep in mind the observed chromium evaporation (see section below), which leads to a lower observed mass gain for the uncoated samples. A detailed discussion of the combination of mass gain with chromium evaporation, taking into account the cobalt oxidation, can be found in our previous publication [1].

#### 3.2. Chromium evaporation

The evaporation of chromium from the cerium cobalt coated samples is plotted in Fig. 2, where the uncoated substrate material was added for comparison. The amount of the evaporated chromium was reduced by approximately 90% compared to the

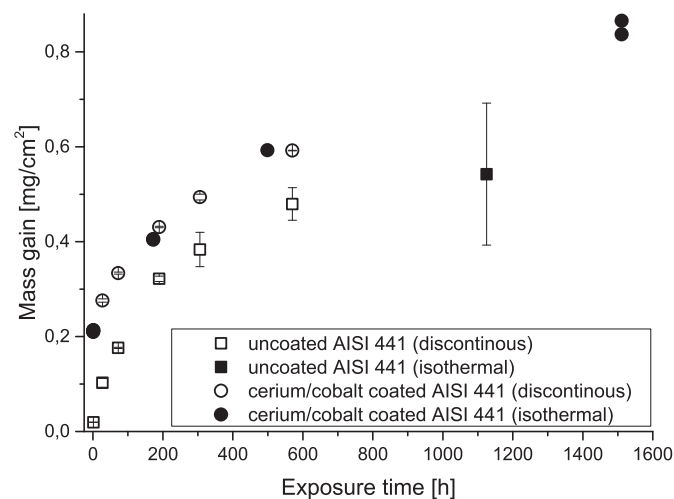


Fig. 1. Mass gain of Ce/Co coated AISI 441 compared to the uncoated substrate material (discontinuous exposed samples are represented by hollow symbols and isothermal exposed samples are represented by filled samples) adapted from Ref. [1].

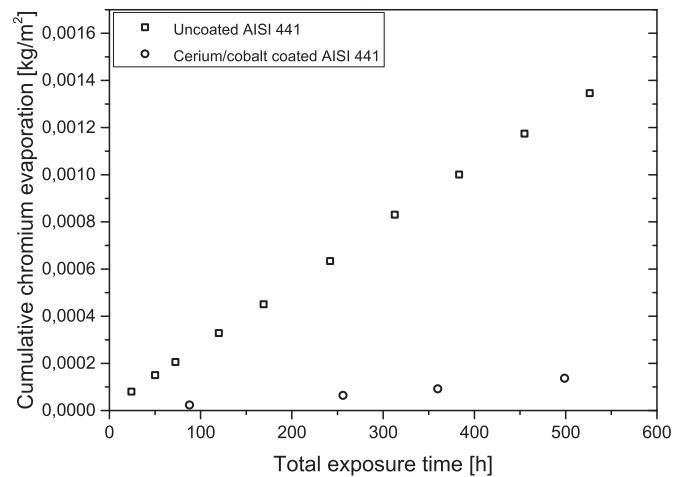


Fig. 2. Cumulative chromium evaporation of cerium/cobalt coated AISI 441 compared to uncoated material adapted from Ref. [1].

uncoated material. Both curves followed a linear trend. The uncoated material evaporated a total mass of about 0.0014 kg/m<sup>2</sup> chromium after 526 h of exposure. The cerium/cobalt coated material showed a drastically reduced chromium evaporation of about 0.00014 kg/m<sup>2</sup> after about 500 h exposure time.

#### 3.3. Area specific resistance

The area specific resistance was measured in two ways: ex-situ – meaning with different pre-oxidation times and short measurement times and in-situ where the electrodes were directly applied on a 60 min pre-exposed sample and then continuously for 500 h measured at 850 °C.

The measured ASR values for one oxide scale are plotted in Fig. 3, i.e. half the value measured for the sample. The in-situ measurement was carried out for about 500 h and the ASR measurement was interrupted for about 75 h after an exposure time of 130 h due to a failure in the characterization setup, but the setup was not cooled down during that time. The sample was cooled down to a minimum of 300 °C in regular intervals in order to measure the ASR at different temperatures and to calculate the

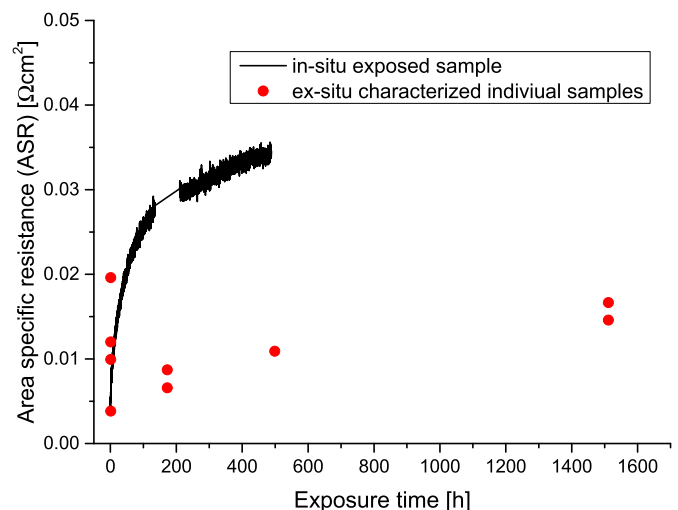


Fig. 3. In-situ and ex-situ ASR evolution over time. Each red circle represents one individual sample.

activation energy. The ASR value of the in-situ characterized sample increased from an initial value of less than  $5 \text{ m}\Omega\text{cm}^2$  to about  $35 \text{ m}\Omega\text{cm}^2$  within 500 h. The ex-situ measured samples showed a large spread for the first measurement point after only 60 min ( $3\text{--}20 \text{ m}\Omega\text{cm}^2$ ), for longer exposure times relatively stable values could be recorded and the increase was rather moderate and a value of about  $15 \text{ m}\Omega\text{cm}^2$  was reached after more than 1500 h.

The development of the activation energy of the in-situ measurement was compared to the ex-situ measured samples and is plotted in Fig. 4. It can be seen that for the ex-situ measured samples the activation energy stays relatively constant in a range of about  $0.55 \pm 0.06 \text{ eV}$  whereas the activation energy of the in-situ measured sample is dramatically increasing from about  $0.55 \text{ eV}$  to  $0.85 \text{ eV}$ .

To relate the measured ASR to the oxidation of the samples, the ex-situ exposed samples mass gain was plotted versus the ASR values (see Fig. 5). The samples exposed for 1 h were excluded from the plot, due to their large spread. It can be seen that a linear correlation between mass gain and ASR value was observed.

### 3.4. Microstructural evolution

As the motivation of this study was the development of a suitable ASR characterization method we focused on the influence of the platinum electrodes on the microstructure. Fig. 6 shows a cross-sectional micrograph and EDX line scans of a coated sample after 500 h of exposure without any electrodes and which has not been ASR characterized, a protective nickel coating had been applied before sample cross-section preparation. An about  $4 \mu\text{m}$  thick double layered oxide layer is clearly visible and also confirmed by the EDX line scan. The inner oxide layer is composed mainly of chromium and oxygen, whereas the outer oxide layer is composed of cobalt, manganese and oxygen.

In Fig. 7 a cross-section of an ex-situ characterized sample with 500 h pre-oxidation is presented. The outer and inner oxide layers, as seen in the case before, are similar in composition, thickness and structure. However, it can be seen a higher concentration of chromium in the outer scale. Additionally one can see the platinum electrode on top of the sample. The EDX line scan does not reveal signs of significant platinum inward diffusion.

Finally in Fig. 8 a micrograph of a 500 h in-situ characterized

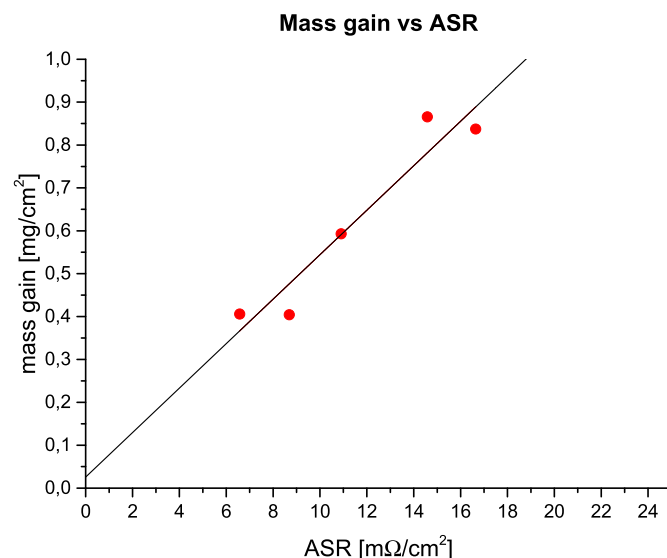


Fig. 5. Ex-situ ASR values versus samples mass gain.

sample is depicted and an EDX line scan plotted. The double layer oxide structure as observed in the two cases before is no longer as distinct and also thickness and composition is drastically different. The oxide scale was about  $20 \mu\text{m}$  thick which is much higher compared to the ex-situ characterized sample. The outer oxide layer is not only much thicker but contains also much more iron and it seems from the EDX line scan that the outer oxide is composed of several layers. Only the inner oxide layer is comparable in thickness and composition; chromium and oxygen. The porous platinum electrode on top of the oxide scale has a bigger grain structure than on the ex-situ measured sample. The bright spots within the oxide scale are not due to platinum inward diffusion and are rather a sample preparation artifact, as the samples have been polished by silica particles.

## 4. Discussion

### 4.1. Corrosion and chromium evaporation

The uncoated material did not fulfill the requirements for a successful application as interconnect material. The resistance to corrosion is not given due to the observed massive spallation of the oxide scale. Additionally too much chromium is evaporated when exposed to humid air. This will lead in the long run lead to chromium depletion in the steel and cathode poisoning [1].

Both the rate of corrosion and the evaporation of chromium were significantly reduced by the application of the double layer coating of  $10 \text{ nm}$  cerium and  $630 \text{ nm}$  cobalt. Initial mass gain of about  $0.21 \text{ mg}/\text{cm}^2$  is due to the conversion of the metallic cobalt to a  $\text{Co}_3\text{O}_4$ . This was already reported in previous works [1,27,28]. The inner coating of cerium is preventing the spallation of the oxide scale successfully, which might be due to a decrease in growth stresses [1]. The outer cobalt coating acts as chromium barrier after conversion to  $\text{Co}_3\text{O}_4$  which then converts to  $(\text{Co:Mn})_3\text{O}_4$  [1]. For the observed time frame only a slightly decreasing rate of chromium evaporation was observed, which however resulted in an almost linear graph for chromium evaporation of both the uncoated and also the cerium cobalt coated samples. This is in the case of the cobalt coated samples due to the rapid oxidation of the cobalt coating to a  $\text{Co}_3\text{O}_4$  cap layer which prevents the outward diffusion of chromium. During the exposure manganese diffuses outwards,

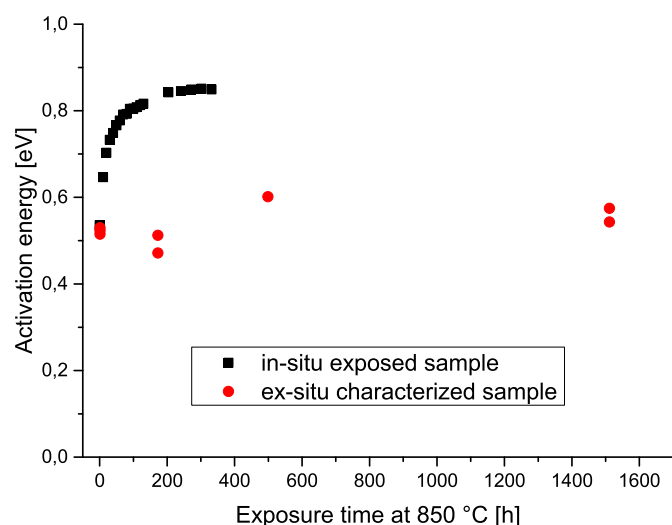


Fig. 4. In-situ and ex-situ activation energy ( $E_a$ ) evolution over time. Each red circle represents one individual sample. (For interpretation of the references to color in this figure legend, the reader is referred to the web version of this article.)



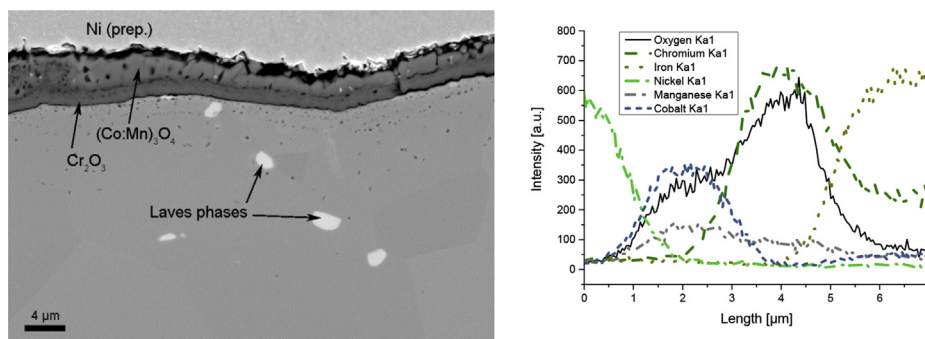


Fig. 6. Cross-sections of sample not ASR characterized exposed for 500 h at 850 °C, including EDX line scan adapted from Ref. [1].

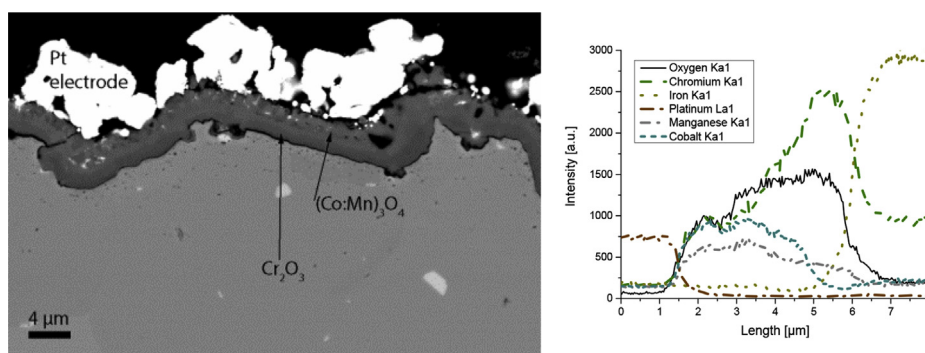


Fig. 7. Cross-sections of sample ex-situ ASR characterized exposed for 500 h at 850 °C, including EDX line scan.

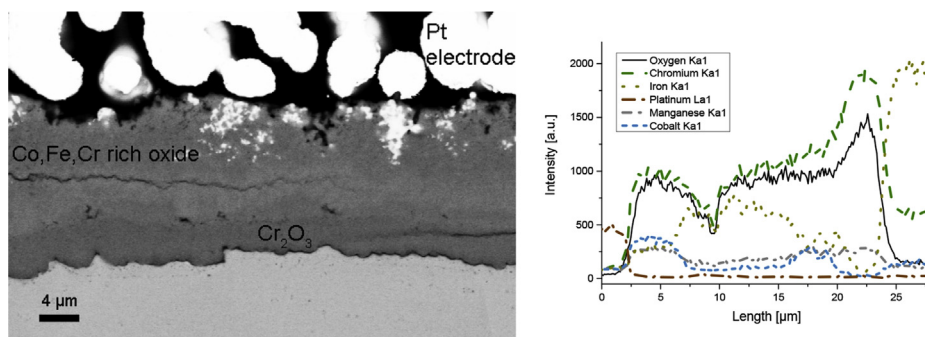


Fig. 8. Cross-sections of sample in-situ ASR characterized exposed for 500 h at 850 °C, including EDX line scan.

leading to the formation of a cobalt manganese spinel [1,27]. The diffusion through this spinel is only slightly lower than the cobalt oxide, thus only a slight decrease in evaporation is observed.

#### 4.2. ASR characterization

The area specific resistance values for both the ex-situ and also the in-situ characterized samples resulted in an approximately parabolic graph (See Fig. 3). Since the mass gain of the coated samples after the initial oxidation step followed an almost parabolic trend, the electronic properties are expected to follow a similar trend as these are mainly dependent on oxide thickness and composition [14]. In our previous investigations we examined the oxide scale evolution of ferritic stainless steels coated with cerium and cobalt and we revealed that the oxide composition for the investigated time frame (up to 1500 h) stays relatively constant [1,27,28]. The outer cobalt manganese spinel layer becomes enriched with manganese and the inner chromium oxide layer

mainly grows in thickness but does not significantly change in composition. Hence a relatively moderate increase in ASR value would be expected, mainly caused by the growing chromia layer. The in-situ measured sample increases within the measurement time of 500 h by more than a factor of 8. The ASR values of the ex-situ measured samples in contrast follow the mass gain in a linear relationship, see Fig. 5.

There is a very large spread in literature ASR values for cobalt manganese coated ferritic stainless steels and, due to the different exposure temperatures, preparation methods and ASR characterization methods, it is hard to find comparable data. Most researchers report values in the range of 5–25 mΩ cm<sup>2</sup> after similar exposure times and temperatures [9,29,30]. Additional complications in comparing these values are attributed to the fact that only very few publications include activation energies for the electron conduction process. Some publications even report on a decreasing ASR evolution over time, which is contradictory to the fact of a growing oxide scale [23,30,31]. One might suspect the extreme

increase of ASR values for the in-situ measured sample was due to the cooling down cycles during the experiment, but the same effect of dramatic increase of ASR was observed for an isothermal measured sample, thus the dramatically increasing ASR is most likely not due to thermal cycling. It can also be excluded to be an effect of the applied current, the measurement was only done during very limited time of the experiment and the 75 h breakdown of the electronic measurement observed after 130 h of exposure lead to the suspicion that the effect was caused by something else, such as platinum interaction. Findings on increased oxidation under the influence of current such as reported by Kawamura et al. and Kodjamanova et al. are not considered as applicable here, since the measurement time was only very short (less than 0.1%) compared to the overall exposure time [32,33].

As mentioned above, one can assume an almost linear dependency between ASR values and mass gain in cases where the oxide layer does not drastically change in composition and ratio between outer and inner oxide scale thickness. Fig. 5 shows the link between mass gain and ASR values. Although the increase in ASR is slightly higher than expected, one can justify the faster increase by a higher ratio of chromium oxide in the scale, which is less conductive than cobalt manganese spinels [34]. The ASR values of the ex-situ measured samples can be therefore considered to be mainly caused by the double layered oxide and not by the used electrodes.

Furthermore, all samples have been also measured during the cool down at distinct temperature steps to calculate the activation energy for the electronic conduction. The evolution of the activation energy (see Fig. 4) not only clearly shows the expected semi-conducting behavior but also shows that the electron conduction process is time independent for the ex-situ measured samples. The observed values of 0.47 eV–0.62 eV are in the range of theoretical values for thermally grown chromia 0.55 eV and are slightly lower than the value for cobalt manganese coated ferritic steels, reported by Molin et al. and Kruk et al. with an activation energy of 0.75 eV and 0.67/0.70 eV respectively [9,17,35–37]. The slightly lower activation energy might be caused either by impurities in the oxide scale or by doping caused by the cerium in the coating. These results are in line with the expectations one would have based on the microstructural evolution. In contrast to the ex-situ measured samples the activation energy of the in-situ measured sample drastically increases after very short exposure times, which again leads to the suspicion that the measurement or the electrodes influences the oxidation. As seen in the EDX analysis, the outer oxide layer is much thicker and contains much higher amounts of iron. This might have caused the higher activation energy and ASR values.

The microstructural investigation finally revealed a much thicker oxide scale for the in-situ measured sample compared to the ex-situ (and also not ASR characterized) samples. The application of platinum paste on the oxide surface might catalyze the oxidation of the samples during longer exposure times. Since the ASR of the samples was increasing even during the measurement break after 75 h, it can be excluded to be a result of the applied measurement current. However, in-situ measurements of the area specific resistance with platinum electrodes are very common. One might suspect a milder influence for samples with longer pre-oxidation times when measured in-situ but, based on our findings in this study, one cannot exclude effects of the platinum electrodes on the oxidation during long term experiments. The ex-situ measured samples in contrast showed no drastic change in microstructure and were considered to be non-influenced by the measurement. These samples furthermore showed a linear relationship between mass gain and ASR values, which is in-line with the underlying theory.

## 5. Conclusion

A method for the characterization of the area specific resistance of metallic interconnect materials was developed, which allows to investigate the evolution of ASR values and activation energy in an ex-situ process. A linear dependency was observed for the ASR values on mass gain data – thus oxide scale thickness. The ex-situ measured samples showed furthermore activation energies for the electron conduction process in the range of  $0.55 \pm 0.06$  eV. It could be proven that in-situ measurement with platinum electrodes leads to increased oxidation and unreliable data. Microstructural investigations after these measurements showed a dramatic increase in oxide scale thickness and lead to significant compositional changes for in-situ measured samples. Due to the observed interaction of the platinum electrodes with the oxide scale a long term measurement with this kind of electrodes is not recommended.

## Acknowledgments

Sandvik Materials Technology AB is acknowledged for providing the samples. The financial support received from The Swedish Research Council and Swedish Energy Agency (Grant Agreement No 34140-1), The Swedish High Temperature Corrosion Centre as well as the Nordic NaCoSOFC project is gratefully acknowledged. Furthermore, the funding received from the European Union's Seventh Framework Programme (FP7/2007-2013) for the Fuel Cells and Hydrogen Joint Technology Initiative under grant agreement n° [278257] is thankfully acknowledged.

## References

- [1] J.G. Grolig, J. Froitzheim, J.E. Svensson, J. Power Sources 248 (2014) 1007–1013.
- [2] F. Mauvy, J.M. Bassat, E. Boehm, J.P. Manaud, P. Dordor, J.C. Grenier, Solid State Ion. 158 (2003) 17–28.
- [3] M.V.F. Schlupp, B. Scherrer, H. Ma, J.G. Grolig, J. Martynczuk, M. Prestat, L.J. Gauckler, Phys. Status Solidi A-Appl. Mat. 209 (2012) 1414–1422.
- [4] R. Sachitanand, M. Sattari, J.E. Svensson, J. Froitzheim, Int. J. Hydrog. Energy 38 (2013) 15328–15334.
- [5] D.E. Alman, P.D. Jablonski, Int. J. Hydrog. Energy 32 (2007) 3743–3753.
- [6] M. Stanislawski, J. Froitzheim, L. Niewolak, W.J. Quadakkers, K. Hilpert, T. Markus, L. Singheiser, J. Power Sources 164 (2007) 578–589.
- [7] P.D. Jablonski, C.J. Cowen, J.S. Sears, J. Power Sources 195 (2010) 813–820.
- [8] I. Belogolovsky, P.Y. Hou, C.P. Jacobson, S.J. Visco, J. Power Sources 182 (2008) 259–264.
- [9] X. Chen, P.Y. Hou, C.P. Jacobson, S.J. Visco, L.C. De Jonghe, Solid State Ion. 176 (2005) 425–433.
- [10] W.J. Quadakkers, J. Piron-Abellan, V. Shemet, L. Singheiser, Mater. High. Temp. 20 (2003) 115–127.
- [11] J.W. Fergus, Int. J. Hydrog. Energy 32 (2007) 3664–3671.
- [12] J. Froitzheim, H. Ravash, E. Larsson, L.G. Johansson, J.E. Svensson, J. Electrochem. Soc. 157 (2010) B1295–B1300.
- [13] J.G. Grolig, H. Abdesselam, M. Gas, H.F. Windisch, J. Froitzheim, J.E. Svensson, ECS Trans. 57 (2013) 2339–2347.
- [14] W.Z. Zhu, S.C. Deevi, Mater. Res. Bull. 38 (2003) 957–972.
- [15] S. Megel, E. Girdauskaite, V. Sauchuk, M. Kusnezoff, A. Michaelis, J. Power Sources 196 (2011) 7136–7143.
- [16] K. Huang, P.Y. Hou, J.B. Goodenough, Mater. Res. Bull. 36 (2001) 81–95.
- [17] S. Molin, B. Kusz, M. Gazda, P. Jasinski, J. Solid State Electrochem. 13 (2009) 1695–1700.
- [18] P. Wei, X. Deng, M.R. Batani, A. Petric, Corrosion 63 (2007) 529–536.
- [19] I. Antepara, I. Villarreal, L.M. Rodriguez-Martinez, N. Lecanda, U. Castro, A. Laresgoiti, J. Power Sources 151 (2005) 103–107.
- [20] B. Hua, J. Pu, F. Lu, J. Zhang, B. Chi, L. Jian, J. Power Sources 195 (2010) 2782–2788.
- [21] S. Fontana, R. Amendola, S. Chevalier, P. Piccardo, G. Caboche, M. Viviani, R. Molins, M. Sennour, J. Power Sources 171 (2007) 652–662.
- [22] P. Piccardo, P. Gannon, S. Chevalier, M. Viviani, A. Barbucci, G. Caboche, R. Amendola, S. Fontana, Surf. Coatings Technol. 202 (2007) 1221–1225.
- [23] M.R. Ardigo, I. Popa, S. Chevalier, V. Parry, A. Galerie, P. Girardon, F. Perry, R. Laucournet, A. Brevet, E. Rigal, Int. J. Hydrog. Energy 38 (2013) 15910–15916.
- [24] A.W.B. Skilbred, R. Haugsrud, J. Power Sources 206 (2012) 70–76.
- [25] J. Puranen, M. Pihlatie, J. Lagerbom, G. Boleili, J. Laakso, L. Hyvarinen, M. Kymälähti, O. Himanen, J. Kiviahio, L. Lusvarghi, P. Vuoristo, Int. J. Hydrog.

- Energy 39 (2014) 17284–17294.
- [26] X. Montero, N. Jordan, J. Piron-Abellan, F. Tietz, D. Stover, M. Cassir, I. Villarreal, J. Electrochem. Soc. 156 (2009) B188–B196.
- [27] S. Canovic, J. Froitzheim, R. Sachitanand, M. Nikumaa, M. Halvarsson, L.G. Johansson, J.E. Svensson, Surf. Coatings Technol. 215 (2013) 62–74.
- [28] J. Froitzheim, S. Canovic, M. Nikumaa, R. Sachitanand, L.G. Johansson, J.E. Svensson, J. Power Sources 220 (2012) 217–227.
- [29] Z. Yang, G. Xia, S.P. Simner, J.W. Stevenson, J. Electrochem. Soc. 152 (2005) A1896–A1901.
- [30] K.O. Hoyt, P.E. Gannon, P. White, R. Tortop, B.J. Ellingwood, H. Khoshuei, Int. J. Hydrog. Energy 37 (2012) 518–529.
- [31] Z.G. Yang, G.G. Xia, C.M. Wang, Z.M. Nie, J. Templeton, J.W. Stevenson, P. Singh, J. Power Sources 183 (2008) 660–667.
- [32] K. Kawamura, T. Nitobe, H. Kurokawa, M. Ueda, T. Maruyama, J. Electrochem. Soc. 159 (2012) B259–B264.
- [33] P. Kodjamanova, Q.X. Fu, L. Gautier, Oxid. Met. 79 (2013) 53–64.
- [34] X.H. Deng, P. Wei, M.R. Bateni, A. Petric, J. Power Sources 160 (2006) 1225–1229.
- [35] A. Petric, H. Ling, J. Am. Ceram. Soc. 90 (2007) 1515–1520.
- [36] J.H. Park, K. Natesan, Oxid. Met. 33 (1990) 31–54.
- [37] A. Kruk, M. Stygar, T. Brylewski, J. Solid State Electrochem. 17 (2013) 993–1003.